Journal of Sciences, Islamic Republic of Iran 25(1): 35 - 49 (2014) http://jsciences.ut.ac.ir
University of Tehran, ISSN 1016-1104

Petrological Evolution of the Upper Mantle Beneath the Southern Sanandaj-Sirjan Zone: Evidence from Kuhshah Peridotite Massif, Southeast Iran

H. Ahmadipour*, and J. Shahabpour

Department of Geology, Faculty of Sciences, Shahid Bahonar University of Kerman, Kerman,Islamic Republic of Iran

Received: 24 February 2014/ Revised: 7 April 2014/ Accepted: 29 April 2014

Abstract

The Kuhshah ultramafic complex is located in the south-east of Sanandaj-Sirjan metamorphic zone, near the probable remnants of Neotethys plate in Iran. It consists of highly depleted harzburgites, dunites, chromitite bands and altered gabbros. The ultramafic parts have been intruded by numerous clinopyroxenite dykes and veins. In the harzburgites, there are different generations of olivine, orthopyroxene and spinel. The chemical composition of the first generation minerals indicates that the harzburgites are depleted in incompatible elements, but the other generations show melt/rock interaction features which can be found in a suprasubduction zone setting. During subduction of the Neotethys plate beneath the Sanandaj-Sirjan zone, a back arc basin developed between the Sanandaj-Sirjan arc and the central Iranian microcontinent. Whole rock and mineral chemistry, specially, cromespinels, show that the harzburgites formed underneath this basin. After depletion, ascending melts with boninitic compositions reacted with these peridotites to form dunites and chromitite bands. The updoming and decompression of the mantle in the next stage, led to remelting at deeper levels and development of clinopyroxenite parental melts which intruded into the uppermost mantle. Then, the new basin closed and the Kuhshah peridotites were emplaced in present position.

Keywords: Iran; Melt/peridotite reaction; Suprasubduction zone setting; Clinopyroxenite.

Introduction

Peridotite complexes in orogenic belts, provide clues on the evolution of the lithospheric mantle. These peridotites have been emplaced in many metamorphic terrains in the root zones of mountain belts [10]. Most of them intruded into metamorphosed continental crustal rocks as discrete lensoid masses or as a part of ophiolitic mélange along major sutures. Several peridotite massifs such as Sorkh Band, Band-e-Ziarat, and Kuhshah (this study), were tectonically emplaced in

* Corresponding author: Tel/Fax: +983413222035; Email: hahmadipour@yahoo.com

Sanandaj-Sirjan zone as a part of the ophiolite mélange (Fig. 1) and some of them have been studied earlier [44,45,48,18,30,16,33].

This study presents field, structural, mineralogical and geochemical data on the Kuhshah complex in order to determine its mode of formation. The study of Kuhshah complex reveals some features of Neotethyian remnants and highlights the occurrence of melt/peridotite reaction processes in this part of Iranian upper mantle.

Geological setting

The Kuhshah complex with a dimension of 18 km by 5 km has been tectonically emplaced in the Bajgan metamorphic complex ([30]; Pzsh in Fig. 1), 40 km north-west of the town of Kahnuj, in Kerman province of Iran (Fig. 1). This complex is one of the numerous peridotite masses that have been tectonically emplaced in southern Sanandaj-Sirjan zone. Sabzehei [44,45] stated that the ultramafic complexes are polygenetic bodies generated by differentiation and crystallization of ultramafic magmas. McCall [30] considered these massifs as parts of mélange of southern Sanandaj-Sirjan/ Bajgan-Durcan (SS/BD) microcontinent sliver, but he did not give any comment on the Kuhshah massif.

In the light of structural data and isotope age dating on Band-e-ziarat ophiolite, which is located at 35 km southeast of Kuhshah [18], and after the invaluable structural and geochemical studies of McCall [30] and Sengor, [48], Ghasemi and Talbot [16] concluded that the Band-e ziarat ophiolite may be considered to be the remnant of the Naien-Baft Ocean. Shahabpour [51] showed that the Sanandaj-Sirjan magmatic arc including the Siahkuh batholith and the ShahrBabak-Baft ensimatic back arc basin, were formed over the northern steeply dipping Neotethyan subduction zone during late Triassic to late Cretaceous.

Materials and Methods

Major elements in whole rocks were analysed by inductivity coupled plasma atomic emission spectrometry (ICP-AES) at the laboratory of ALSCHEMEX in Canada. Minor and trace elements in whole rocks were analysed by solution-ICP-MS (mass spectrometry at the same laboratory.

Electron microprobe analyses reported here were performed on a GEOL JXA, 8900, superprobe in the Münster university microprobe laboratory (Germany), using an accelerating voltage of 15 kv a focused beam of 15 nA and counting times of 20-30 s against natural mineral standards.

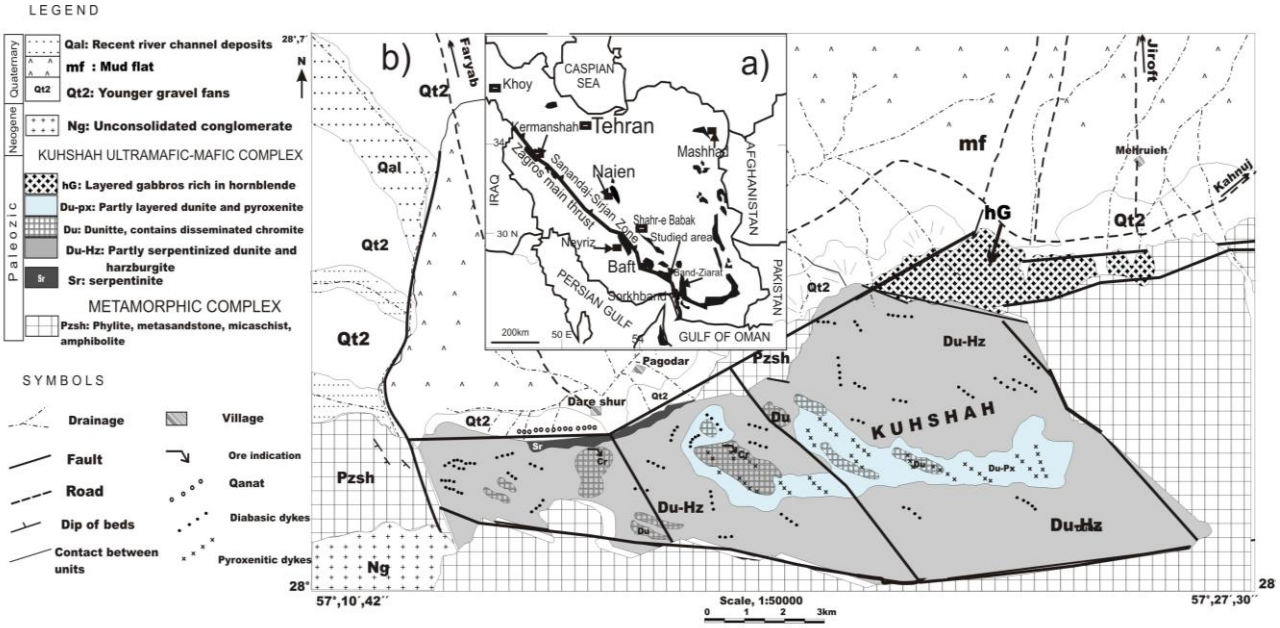

Figure. 1. Geological map of Kuhshah peridotite massif (b). Inset (a) shows the location of Kuhshah in south-east Iran

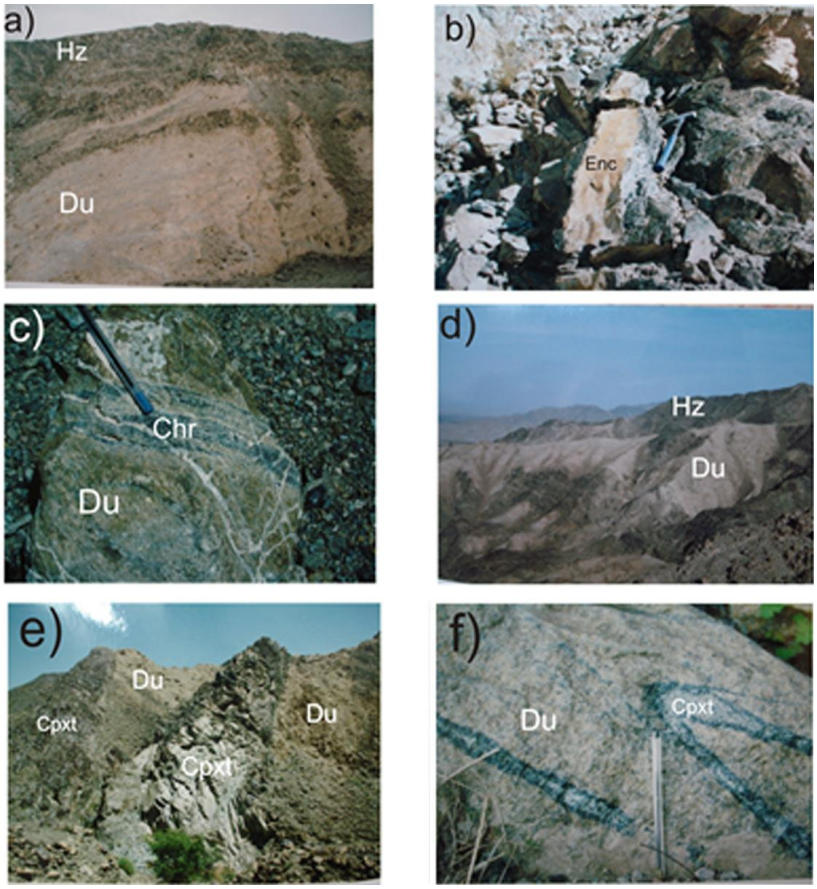

Figure 2. a**)** Diffuse modal layering of harzburgites (Hz) and dunites (Du) in Kuhshah; b) Metamorphosed carbonaceous enclave in Kuhshah peridotites; c) Thin chromitite bands in Kuhshah dunites; d) Lensoid and irregular dunites in Kuhshah; e) Straight discontinuous set of pyroxenite bands in Kuhshah dunites and f) Folded pyroxenite band in Kuhshah peridotites. Enc: Metamorphosed calcareous enclave, Chr: Chromitite bands and Cpxt: Clinopyroxenites.

Results

Field characteristics of the Kuhshah peridotite massif

In the Kuhshah massif, harzburgites dominate and host other lithologies (Hz in Fig. 1) and show a weak foliation which is evidenced by alignment of orthopyroxene and spinel grains. The layering of harzburgites and dunites (Fig. 2a) and dominant foliation are commonly parallel. Kuhshah peridotites contain metamorphosed lens-shaped calcareous enclaves up to 40 cm wide and 3 m long (Fig. 2b). They are fine-grained and contain diopsidic clinopyroxenes (up to 0.5 mm), calcite, epidote, a lot of fine-grained opaque minerals and unhedral garnet (grossular) grains. Dunites in Kuhshah massif occur as layers (Fig. 2a) and irregular bodies, which do not show foliation (Du in Fig. 1). In layered-shaped dunites, the transition between dunites and harzburgites is marked by gradational appearance of orthopyroxene in the harzburgites, while the contact between dunitic patches and hosted harzburgites is completely abrupt and irregular. The dunites (Du in Fig. 1) contain accessory Cr-spinel grains and in some places chromitite bands (up to 5 cm in thickness) (Fig. 2c) that are concordant with respect to the dunite-harzburgite banding. Chromitites have preserved their magmatic features without any deformation textures and consist of about 60 – 80 modal % chromite with gradational contacts to the host dunites. Lensoid, patchy and irregular dunites (up to 300 m in diameter) are located in the central parts of the massif (Fig. 2d).

Always in this area, there are numerous clinopyroxenite veins and dykes cutting the dunites (Du-Px in Fig. 1). These intrusives with sharp and serpentinized contacts, mainly comprise coarse-grained clinopyroxene (5 mm in average) and fine-grained olivine. Different shapes of discontinuous pyroxenitic veins up to 10 cm thickness (Fig. 2e and 2f) are

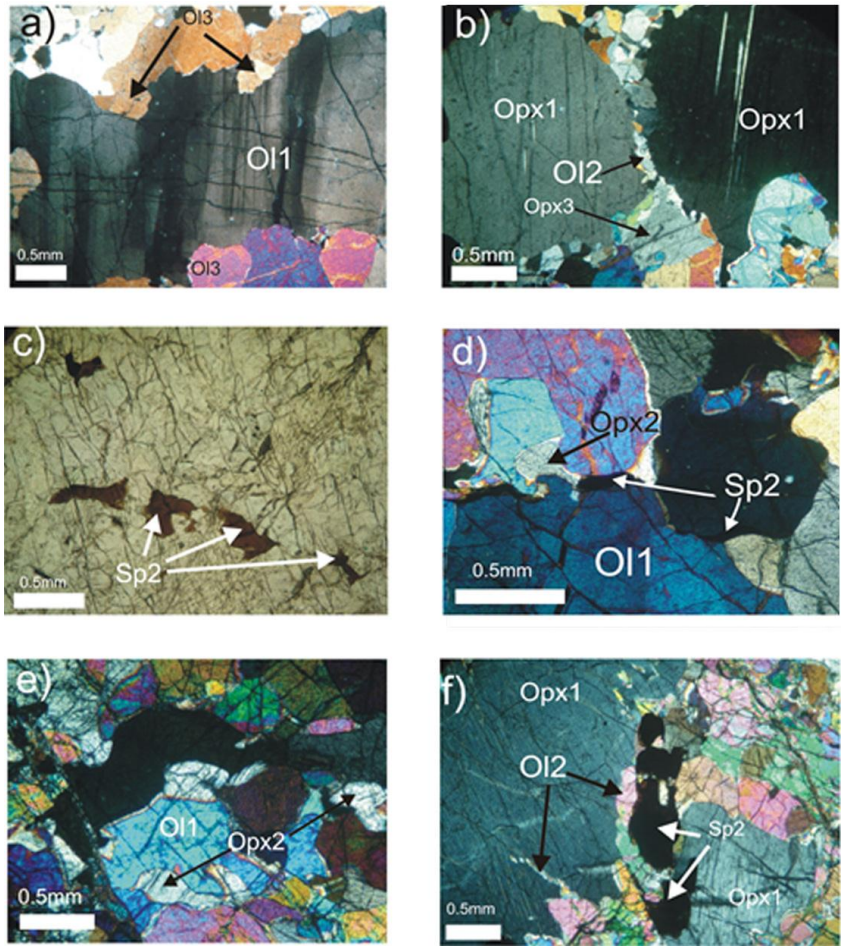

Figure. 3. Microstructures of Kuhshah peridotites: a) First (Ol1) and second (Ol2) generations of olivines in Kuhshah harzburgites; b) First generation semirounded porphyroclastic orthopyroxenes (Opx1) with a trail of olivine neoblasts (Ol2) and small undeformed third generation orthopyroxenes (Opx3); c) Alignment of Sp2 in impregnated harzburgites; d) Strain free, interstitial Sp2 and orthopyroxene (Opx2) between Ol1 and Opx1 in harzburgites; e) Interstitial orthopyroxene (Opx2) between the first generation grains; f) Unstrained olivines (Ol2) and spinel (Sp2) between the first generation orthopyroxene grains (Opx1).

distributed throughout the dunites. Some show a parallel set of veins (Fig. 2e) in the host rocks. There is a black, coarse to fine-grained and highly amphibolitized gabbro in the south-eastern part of Kuhshah complex (hG in Fig. 1). It is compositionally and texturally heterogeneous and contains many leucocratic veins bounded by irregular boundaries without chilled margin. The Kuhshah complex is crosscut by diabase dykes of up to 5m thick. They are devoid of high temperature or high pressure deformation textures.

Petrography

As illustrated in Table 1, in Kuhshah peridotites, different generation of minerals with distinct petrographic features can be observed. Generally, the first generation ones (Ol1, Opx1 and Sp1) show some features such as porphyroclastic textures, elongation, kinking and orientation that indicate these minerals may be primary phases, which have been experienced high P-T deformation in the mantle conditions.The second ones crystallized as interstitial phases, whereas the third generation ones produced by recrystallization of the first and second generation minerals.

The first generation olivines (Ol1) are internally deformed porphyroclastic crystals with irregular grain edges (Fig. 3a), but the second generation ones (Ol2) have been crystallized as trails of small grains in or at the boundaries of Opx1 and Ol1 (Fig. 3b and 3f). This type of olivine is characteristic of Kuhshah impregnated harzburgites. The third generation olivines (OL3)

Table 1. Petrographical characteristics of kuhshah rocks. Ol1: First generation olivines, Ol2: Second generation olivines, Ol3: Third generation olivines, Opx1: First generation orthopyroxene, Opx2: Second generation orthopyroxene, Opx3: Third generation orthopyroxene, Sp1: First generation spinel, Sp2: Second generation spinel, Cpx: clinopyroxene

Rock type	Overal texture	Modal composition		Volume percent	Size (mm)	Mineral textures	Compositional features
Harzburgites	Nonequigranular and Porphyroclastic	Ol (60-85 Vol.%)	Ol1	40-60	Up to 10	Internally deformed porphyroclastic crystals with irregular grain edges (Fig. 3a)	Av. fo no: 0.927
			OL2	5	0.2	As trails of grains in or at the boundaries of Opx1 (Fig. 3b)	Av. fo no: 0.9
			Ol3	10-15	0.5	Undeformed polygonal neoblasts which surround Ol1 (Fig. 3a)	Av. fo no: 0.92
		Opx (15-30 Vol%)	Opx1	10-20	Up to 10	Semi-rounded to elongated porphyroclastic grains with lobate contacts (Fig. 3b) , contain Cpx lamellae and olivine neoblasts (Ol2).	Av. mg no: 0.914
			Opx2	2	0.2	Undeformed irregular interstitial grains located between Ol1 and Opx1 (Fig. 3d and 3e).	Av. mg no: 0.9
			Opx3	5	0.4	Undeformed polygonal neoblasts which surround Opx1 (Fig. 3b).	Av. mg no: 0.9
		Sp (2 vol.%)	Sp1	1.5	2	Brown subidiomorphic or irregular grains with pullapart fractures.	Av. Cr#: 70.5
			Sp2	0.5	0.5	Anhedral interstitial greenish grains placing between the first generation olivines and orthopyroxenes (Fig. 3c).	Av. Cr#: 33.5
		Cpx (0.5%)		0.5	1	Deformed interstitial grains	
Dunites	Granular	Ol		98	Up to 15	Deformed and undeformed grains with lobate and straight boundaries	Av. fo#: 0.8
		Sp		2	2	Rhomb-shaped undeformed dark disseminated grains generally located at the olivine grain boundaries	Av. Cr#: 74.7
Chromitites	Cumulate	Ol		Up to 20	3	Undeformed intercumulus phases between chromite grains	Av. fo#: 0.925
		Sp		Up to 80	6	Partially fractured cumulus phases	Av. Cr#: 0.815
Clinopyroxenites	Cumulate	Cpx		Up to 90	10	Coarse cumulus phases sometimes with Opx exsolution lamellae	Av. Mg#: 0.9
		Ol		Up to 10	3	Unstrained intercumulus grains	Av. fo#: 0.82

represent undeformed polygonal neoblasts which surround Ol1 (Fig. 3a). The first generation orthopyroxenes (Opx1) are semi-rounded to elongated porphyroclastic grains with lobate contacts (Fig. 3b). They contain Cpx lamellae and olivine neoblasts (Ol2). The second generation ones (Opx2) shows undeformed irregular interstitial grains which crystallized between OL1 and Opx1 (Fig. 3d and 3e). The third generation orthopyroxenes (Opx3) represent undeformed polygonal neoblasts which surround Opx1 (Fig. 3b). The first generation spinels (Sp1) are brown subidiomorphic or irregular shapes with pull apart fractures that set in or at the contacts of olivines, but the second generation ones (Sp2) crystallized between Ol1-Ol1 or Ol1-Opx1 contacts (Fig. 3c and 3f), sometimes forming pseudo-veins (Fig. 3c). They represent anhedral interstitial greenish grains placing between the first generation crystals. These pseudo-veins in the impregnated host harzburgites possibly mark the paths of migrating melts from which Sp2 have crystallized. In the harzburgites, contacts between Ol1-Ol1 and Ol1-Opx1, (Table 1) are curved and some orthopyroxene porphyroclasts show lobate boundaries and olivine neoblasts (Ol2) are found in their embayments. Two shapes of dunites in Kuhshah show similar petrographic features and their undeformed rhomb-shaped spinels are located at the grain boundaries or set as inclusion in olivines.

Textural relationships between different generation minerals (Table 1) show that the first generations are refractory and -primary minerals, while the second generation phases resulted from melt/peridotite reactions at upper mantle conditions. Some primary minerals have been overprinted by the second generation phases due to above reactions. Polygonal-undefomed crystals of the third generation minerals, show that they probably, recrystallized as the last generation phases.

Mineral chemistry

Olivine

Table 2 shows representative olivine analyses from Kuhshah. Unzoned first generation olivines in Kuhshah depleted harzburgites show a narrow range of Fo content (92 to 93), which is different from the values defined by fertile lherzolites and depleted harzburgites [12,4]. There are some variations in NiO wt% (0.36-0.44) but compositionally most of them are similar to mantle olivines. In one sample, the amount of NiO is 0.55 wt%. This may be due to melt/rock reaction processes (as shown by Ishimaru and Arai, 2008). In some impregnated harzburgites (such as sample named KS1), different generation olivines show different compositions, so that in this sample, the forsterite value for Ol1 is 93, while the average value for Ol2 is 90 and for Ol3 is 92. Olivines in Kuhshah dunites contain slightly lower forsterite (0.88-0.90) and NiO (0.19-0.38)

Table 2. Representative analyses of different types of olivines from Kuhshah massif

Sample	Ks2	Ks3	Ks10	Ks1	Ks1	Ks1	Ks1	Ks1	Ks6	Ks6	Ks12	Ks12	Ks19	Ks19	Ks7	Ks7	Ks11	Ks21	Ks21	Ks22	Ks121
Rock	Dunite	Dunite	Dunite	Hz	Hz	Hz	Hz	Hz	Hz	Hz	Hz	Hz	Du-Chr	Du-Chr	Ol-Cpxt	Ol-Cpxt	Ol-Cpxt	Ol-Cpxt	Ol-Cpxt	Ol-Cpxt	Ol-Cpxt
Mineral	Ol	Ol	Ol	Ol1	Ol2	Ol2	Ol3	Ol3	Ol1	Ol3	Ol1	Ol1	Ol	Ol	Ol	Ol	Ol	Ol	Ol	Ol	Ol
SiO2	40.95	41.44	41.91	40.63	41.32	40.44	41.32	41.72	41.26	42.35	41.91	41.15	41.06	41.07	40.28	39.22	39.15	40.89	40.50	40.12	40.20
TiO2	0.00	0.00	0.00	0.01	0.00	0.00	0.00	0.05	0.00	0.00	0.00	0.00	0.01	0.00	0.00	0.00	0.03	0.02	0.00	0.01	0.04
Al2O3	0.00	0.00	0.00	0.00	0.03	0.01	0.03	0.01	0.00	0.08	0.00	0.00	0.00	0.00	0.01	0.00	0.00	0.00	0.00	0.01	0.00
Cr2O3	0.00	0.01	0.00	0.00	0.01	0.07	0.01	0.13	0.00	0.04	0.01	0.00	0.00	0.01	0.00	0.00	0.00	0.00	0.00	0.00	0.00
FeO tot	11.36	10.41	9.53	7.82	8.79	11.40	8.79	8.18	8.26	7.85	7.38	7.79	7.67	8.16	17.52	18.10	17.76	15.31	14.14	17.06	17.01
MnO	0.20	0.24	1.16	0.07	0.11	0.15	0.11	0.04	0.14	0.12	0.07	0.10	0.19	0.12	0.14	0.19	0.29	0.24	0.18	0.24	0.23
MgO	47.74	47.80	47.91	50.42	50.32	46.75	50.32	49.85	50.85	48.96	49.76	50.43	50.30	50.37	42.48	43.07	43.04	43.82	44.16	41.81	42.82
CaO	0.04	0.02	0.00	0.00	0.02	0.07	0.02	0.03	0.00	0.04	0.03	0.00	0.01	0.02	0.00	0.00	0.00	0.00	0.00	0.00	0.00
NiO	0.36	0.38	0.19	0.36	0.34	0.19	0.34	0.14	0.44	0.15	0.55	0.37	0.27	0.42	0.56	0.41	0.60	0.36	0.51	0.63	0.38
Na2O	0.00	0.00	0.00	0.00	0.00	0.00	0.00	0.01	0.00	0.01	0.00	0.00	0.00	0.00	0.00	0.00	0.00	0.00	0.00	0.00	0.00
K2O	0.00	0.00	0.00	0.00	0.00	0.00	0.00	0.02	0.00	0.01	0.00	0.00	0.00	0.00	0.00	0.00	0.00	0.00	0.00	0.00	0.00
Total	100.65	100.30	100.70	99.31	100.94	99.08	100.94	100.15	100.95	99.59	99.71	99.84	99.51	100.17	100.99	100.99	100.87	100.64	99.49	99.88	100.68
Cations (Structual formula on the basis of 4 oxygen)																					
Si	1.01	1.02	1.03	0.99	1.00	1.01	1.00	1.02	0.99	1.04	1.02	1.00	1.00	1.00	1.02	0.99	0.99	1.03	1.02	1.02	1.02
Ti	0.00	0.00	0.00	0.00	0.00	0.00	0.00	0.00	0.00	0.00	0.00	0.00	0.00	0.00	0.00	0.00	0.00	0.00	0.00	0.00	0.00
Al	0.00	0.00	0.00	0.00	0.00	0.00	0.00	0.00	0.00	0.00	0.00	0.00	0.00	0.00	0.00	0.00	0.00	0.00	0.00	0.00	0.00
Cr	0.00	0.00	0.00	0.00	0.00	0.00	0.00	0.00	0.00	0.00	0.00	0.00	0.00	0.00	0.00	0.00	0.00	0.00	0.00	0.00	0.00
Fe3	0.00	0.00	0.00	0.03	0.01	0.00	0.01	0.00	0.03	0.00	0.00	0.01	0.00	0.02	0.00	0.04	0.05	0.00	0.00	0.00	0.00
Fe2	0.23	0.21	0.20	0.13	0.16	0.24	0.16	0.17	0.14	0.16	0.15	0.15	0.15	0.15	0.37	0.34	0.33	0.32	0.30	0.36	0.36
Mn	0.00	0.01	0.02	0.00	0.00	0.00	0.00	0.00	0.00	0.00	0.00	0.00	0.00	0.00	0.00	0.00	0.01	0.01	0.00	0.01	0.00
Mg	1.75	1.75	1.75	1.84	1.81	1.74	1.81	1.81	1.83	1.79	1.81	1.83	1.83	1.82	1.60	1.62	1.62	1.64	1.66	1.59	1.61
Ca	0.00	0.00	0.00	0.00	0.00	0.00	0.00	0.00	0.00	0.00	0.00	0.00	0.00	0.00	0.00	0.00	0.00	0.00	0.00	0.00	0.00
Ni	0.01	0.01	0.00	0.01	0.01	0.00	0.01	0.00	0.01	0.00	0.01	0.01	0.01	0.01	0.01	0.01	0.01	0.01	0.01	0.01	0.01
Na	0.00	0.00	0.00	0.00	0.00	0.00	0.00	0.00	0.00	0.00	0.00	0.00	0.00	0.00	0.00	0.00	0.00	0.00	0.00	0.00	0.00
K	0.00	0.00	0.00	0.00	0.00	0.00	0.00	0.00	0.00	0.00	0.00	0.00	0.00	0.00	0.00	0.00	0.00	0.00	0.00	0.00	0.00
tot. cat.	3.00	2.99	3.00	2.99	2.99	3.00	2.99	3.00	2.99	3.00	2.99	2.99	2.99	2.99	2.99	2.99	2.99	2.99	2.99	2.99	2.99
fo-no	0.88	0.89	0.90	0.93	0.92	0.88	0.92	0.92	0.93	0.92	0.92	0.93	0.92	0.93	0.81	0.83	0.83	0.84	0.85	0.81	0.82

contents (Table 2) relative to the harzburgitic ones. Interstitial olivines from olivine-clinopyroxenites show different chemical composition. They have distinctly lower forsterite and NiO contents (0.81-0.85 and 0.11-0.24 wt% respectively) compared with olivines in Kuhshah dunites and harzburgites. Olivines in the chromitite bands are magnesian (average of 0.925) indicating subsolidus Mg-Fe exchange with chromite [43,60].

Spinel

The compositions of different types of spinels in Kuhshah are listed in Table 3. Sp1 grains in harzburgites have Cr# (Cr/(Cr+Al)) between 0.62 and 0.79, Mg# (Mg/(Mg+Fe)) between 0.38 and 0.65 and TiO_2 content 0.05-0.2 wt%. The compositions of these spinels are similar to those which are refered to as refractory cr-spinels left after partial melting of host peridotites [12]. Table 3 and Figures 4a indicate that

Table 3. Representative analyses of different types of spinels from Kuhshah massif

Sample	Ks1	Ks1	Ks1	Ks1	Ks6	Ks6	Ks6	Ks6	Ks12	Ks12	Ks12	Ks1	Ks1	Ks1	Ks1	Ks6
Rock	Hz	Hz	Hz	Hz	Hz	Hz	Hz	Hz	Hz	Hz	Hz	Hz	Hz	Hz	Hz	Hz
Mineral	Opx1	Opx1	Opx1	Opx1	Opx1	Opx1	Opx1	Opx1	Opx1	Opx1	Opx1	OPx2	Opx2	Opx3	Opx3	Opx3
SiO2	55.42	56.02	55.37	56.21	55.32	56.01	55.76	57.03	55.48	55.86	56.34	57.63	56.60	57.13	57.46	56.85
TiO2	0.14	0.13	0.14	0.13	0.13	0.12	0.15	0.06	0.13	0.15	0.12	0.00	0.04	0.05	0.00	0.04
Al2O3	3.37	3.27	3.07	3.47	3.16	3.56	3.77	2.89	3.32	3.81	3.12	0.78	0.71	1.35	1.61	1.45
Cr2O3	0.55	0.46	0.40	0.56	0.46	0.49	0.52	0.48	0.51	0.44	0.43	0.38	0.41	0.47	0.46	0.37
FeOtot	6.63	6.85	6.59	6.43	6.60	6.16	6.45	6.63	6.73	6.40	6.31	5.78	5.95	5.50	5.37	5.39
MnO	0.14	0.08	0.12	0.11	0.08	0.16	0.12	0.11	0.10	0.09	0.13	0.15	0.09	0.10	0.20	0.12
MgO	33.16	33.05	33.24	33.35	32.90	33.37	33.20	33.81	33.81	33.22	33.46	34.98	35.02	35.21	35.38	34.30
CaO	0.53	0.51	0.41	0.42	0.50	0.47	0.51	0.48	0.50	0.41	0.46	0.60	0.62	0.58	0.66	0.58
Na2O	0.03	0.00	0.02	0.00	0.02	0.01	0.00	0.00	0.00	0.01	0.00	0.03	0.02	0.02	0.02	0.04
K2O	0.00	0.00	0.00	0.00	0.00	0.00	0.00	0.00	0.00	0.00	0.00	0.00	0.00	0.00	0.00	0.01
NiO	0.08	0.05	0.13	0.15	0.10	0.04	0.10	0.09	0.10	0.12	0.06	0.10	0.01	0.05	0.06	0.05
Total	100.05	100.42	99.49	100.83	99.27	100.39	100.58	101.58	100.68	100.51	100.43	100.43	99.47	100.46	101.22	99.20
Cation (Structural formula on the basis of 6 oxygen)																
Si	1.92	1.93	1.92	1.93	1.93	1.93	1.92	1.94	1.90	1.92	1.94	1.97	1.96	1.95	1.95	1.97
Ti	0.00	0.00	0.00	0.00	0.00	0.00	0.00	0.00	0.00	0.00	0.00	0.00	0.00	0.00	0.00	0.00
Al	0.14	0.13	0.13	0.14	0.13	0.14	0.15	0.12	0.13	0.15	0.13	0.03	0.03	0.05	0.06	0.06
Fe+3	0.01	0.00	0.01	0.00	0.00	0.00	0.00	0.00	0.04	0.00	0.00	0.01	0.05	0.03	0.03	0.00
Cr+3	0.02	0.01	0.01	0.02	0.01	0.01	0.01	0.01	0.01	0.01	0.01	0.01	0.01	0.01	0.01	0.01
Fe+2	0.18	0.20	0.18	0.18	0.19	0.18	0.19	0.19	0.15	0.18	0.18	0.15	0.12	0.13	0.13	0.16
Mn	0.00	0.00	0.00	0.00	0.00	0.00	0.00	0.00	0.00	0.00	0.00	0.00	0.00	0.00	0.01	0.00
Mg	1.71	1.70	1.72	1.71	1.71	1.71	1.70	1.72	1.73	1.70	1.72	1.79	1.80	1.79	1.79	1.77
Ca	0.02	0.02	0.02	0.02	0.02	0.02	0.02	0.02	0.02	0.02	0.02	0.02	0.02	0.02	0.02	0.02
Na	0.00	0.00	0.00	0.00	0.00	0.00	0.00	0.00	0.00	0.00	0.00	0.00	0.00	0.00	0.00	0.00
K	0.00	0.00	0.00	0.00	0.00	0.00	0.00	0.00	0.00	0.00	0.00	0.00	0.00	0.00	0.00	0.00
Ni	0.00	0.00	0.00	0.00	0.00	0.00	0.00	0.00	0.00	0.00	0.00	0.00	0.00	0.00	0.00	0.00
En	0.90	0.89	0.90	0.90	0.89	0.90	0.89	0.89	0.91	0.90	0.90	0.91	0.92	0.92	0.92	0.91
Fs	0.09	0.10	0.09	0.10	0.10	0.09	0.10	0.10	0.08	0.10	0.09	0.08	0.06	0.07	0.06	0.08
Wo	0.01	0.01	0.01	0.01	0.01	0.01	0.01	0.01	0.01	0.01	0.01	0.01	0.01	0.01	0.01	0.01
Mg#	0.90	0.90	0.91	0.90	0.90	0.91	0.90	0.90	0.92	0.90	0.90	0.92	0.94	0.93	0.93	0.92

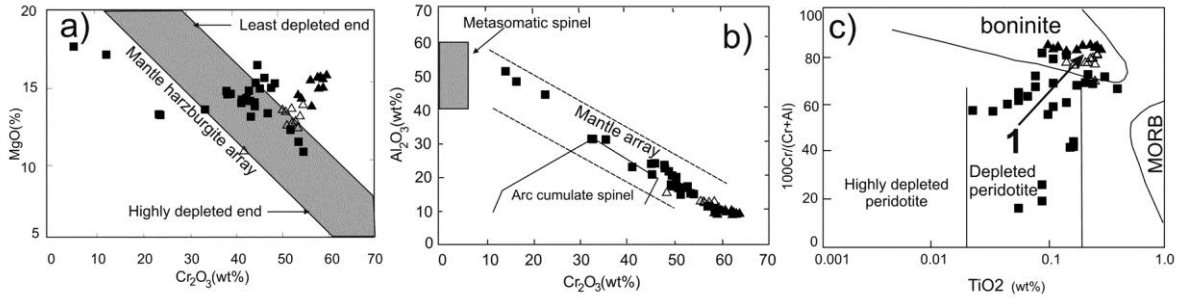

Figure 4. Compositional variations of Kuhshah spinels: a) MgO vs Cr_2O_3. Mantle array is from Al-Aabed (2000); b) Al_2O_3 vs Cr_2O_3. Fields are from Kepezhinskas et al., (1995); c) Cr# vs TiO_2. There is a continuous trend from depleted harzburgitic spinels toward boninite generated dunites and chromitite bands. Fields are from Dick and Bullen (1984) and Arai (1992). Black square: Harzburgites, Black triangle:Cromitite bands, Open triangles:Dunites.

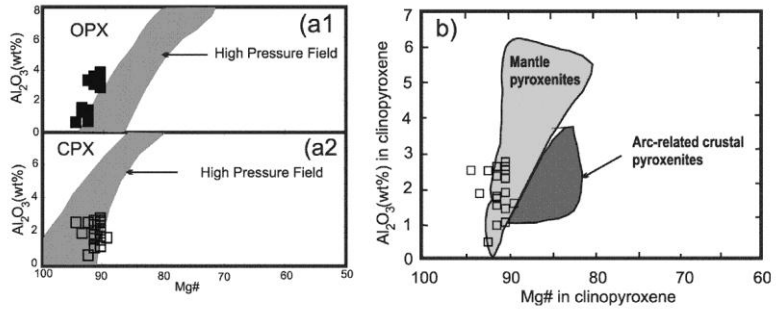

Figure. 5. a1) Variation of Al_2O_3 vs Mg# in Kuhshah orthopyroxenes. a2) Variation of Al_2O_3 vs Mg# in Kuhshah clinopyroxenes. High pressure fields are from Medaris (1972). b) Al_2O_3 vs Mg# in Kuhshah clinopyroxenes. Fields are from Parkinson and Pearce, (1998) and Berly et al., (2006). Symboles are as in Figure 4 and Open square: clinopyroxenites.

these spinels are enriched in Cr and depleted in Mg but these values are consistent with a residual origin for harzburgites. As shown in Table 3, the Sp1 grains are compositionally heterogenous within the same sample. This feature can occur due to impregnation of the peridotites by ascending melts. However, in Figure 4b all of Kuhshah samples plot in the mantle array. Disseminated spinels in dunites have a higher Cr# (0.67-0.78) and TiO_2 contents (0.21-0.24) and show little variation in composition (Fig. 4c). In Figure 4c, they plot in the field of boninite, suggesting that they have been produced by crystallization from boninitic melts. The highest values of Cr# belong to cr-spinel of chromitite bands (Cr# 0.81 to 0.82). In Figure 4c, this type of spinel plots in the field of magmatic chromites that can be formed from boninitic melts at the mantle conditions. In chromitite bands, high Mg# olivines (average Fo is 0.925), high Cr spinels (Cr# is 0.815 in average) and Al_2O_3 contents in spinels (8.96-9.36) are typical of boninitic melts [36], whereas, harzburgitic spinels plot in the field of depleted peridotites in Figure 4c. In this diagram (Fig. 4c), continuous compositional trend 1 from Kuhshah harzburgitic spinels toward those from dunites and chromitits may suggest that boninitic melts from which chromitite bands and dunites are formed, may have reacted with the harzburgites and changed the composition of their spinels toward boninitic spinels.

Interstitial greenish-brown spinels (Sp2) in impregnated harzburgites show a distinctive composition with lower Cr# and NiO values (33.5 and 0.25-0.42 respectively) and higher FeO and Al_2O_3 contents (2.25-4.03 and 31.46-44.76 respectively) in comparison with other spinels. In Fig. 4b and 4c, these Al-rich spinels are separated from the other ones.

Orthopyroxene

Three generations of orthopyroxene in harzburgites are enstatite with almost similar Mg# values (Table 4); but their values for other elements such as Ni, Cr, and Al are different. Primary porphyroclastic orthopyroxenes (Opx1) contain Mg# of 0.90-0.92, Al_2O_3 contents up to 3.56 wt%, and TiO_2 contents of 0.06-0.15 wt%. Interstitial orthopyroxenes (Opx2) contain Al_2O_3 (up to 3.27 wt%), NiO (up to 0.13 wt%), MgO (34-35 wt%), and Cr_2O_3 (up to 0.48) contents. These minerals are enriched in Na_2O (0.02-0.04 wt%), TiO_2 (average 0.13), FeO (up to 6.85) and CaO (0.58-0.66 wt%) contents in relation to the first ones. The chemical compositions of third generation orthopyroxenes (Opx3) are more or less similar to

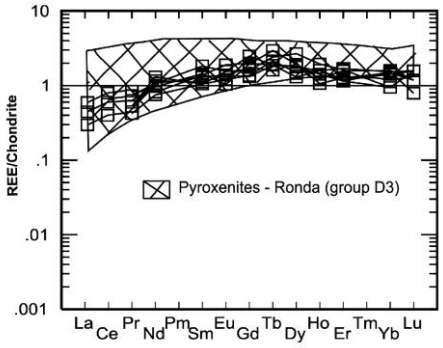

Figure 6. Chondrite normalized whole rock REE patterns for Kuhshah clinopyroxenites that plot in the range of Ronda pyroxenites. Ronda values are from Berly et al. (2006).

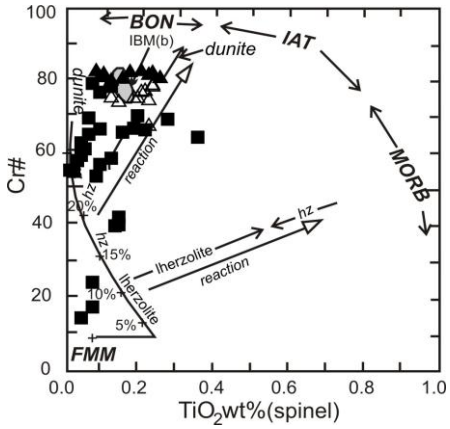

Figure 7. Variations of Cr# vs TiO2. Kuhshah dunites with boninitic chemical nature can be produced by partially melted harzburgites due to interaction of these rocks with boninites. FMM: fertile mantle, IBM(b): Iso-Bonin Mariana with boninitic chemical nature(b). hz: harzburgite, du): dunite. Reference data are from Pearce et al., (2000).

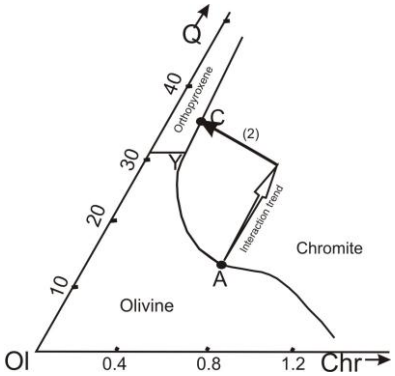

Figure 8. Phase relations in the system Olivine-Quartz-Chromite as determined by Irvine (1977) and modified by Zhou et al., (1996). In Kuhshah, primitive melt (A) may have produced chromite and forsterite-rich olivines along Ol-Chr cotectic. Due to interaction with wall rock peridotites, the melt moved along interaction trend and crystallizes chomitite bands and then, the composition of the melt moves toward orthopyroxene-chromite cotectic (may be along the trend "2") and in upper levels producec these minerals as accessory phases at point "C".

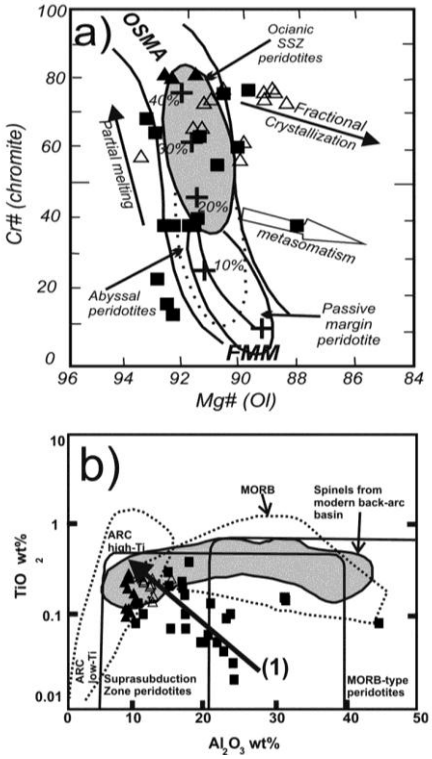

Figure 9. Comparison of Kuhshah peridotites with peridotites from different geological settings: a) Cr# in spinels vs Mg# in coexisting olivines. The field of oceanic suprasubduction zone and passive margin peridotites are from Pearce et al., (2000). OSMA and partial melting trend are from Arai (1994a). FMM: fertile MORB mantle; b) TiO2 vs Al2O3 variations in spinels with respect to modern-day tectonic settings. Fields are from Kamenetsky et al., (2002).

Opx1. In Fig. 5a1, Kuhshah orthopyroxenes plot in the high pressure field orthopyroxenes.

Clinopyroxene

The chemical composition of clinopyroxenes in Kuhshah olivine-clinopyroxenites is shown in Table 5. These minerals are unzoned diopsides and show Mg# values between 0.89 to 0.94, the amount of some oxides such as Cr_2O_3 and Na_2O show great variations and vary from 0.04-0.82 wt% and 0.08-0.27 wt% respectively. In Figure 5a2, Kuhshah samples plot in the field of high pressure clinopyroxenes, while in Figure 5b, these clinopyroxenes show strong affinity toward mantle derived pyroxenites.

Whole rock chemistry

Table 6 shows whole rock chemistry of major rock types in Kuhshah. Major and trace element contents

Table 4. Representative analyses of different types of orthopyroxenes from Kuhshah massif.

Sample	Ks1	Ks1	Ks1	Ks1	Ks1	Ks1	Ks1	Ks1	Ks6	Ks6	Ks6	Ks6	Ks6	Ks12	Ks12	Ks12
Rock	Hz	Hz	Hz	Hz	Hz	Hz	Hz	Hz	Hz	Hz	Hz	Hz	Hz	Hz	Hz	Hz
Mineral	Opx1	Opx1	Opx1	Opx1	Opx1	Opx2	Opx2	Opx3	Opx1	Opx1	Opx2	Opx2	Opx3	Opx1	Opx1	Opx1
SiO2	56.60	57.13	55.42	57.63	57.46	56.02	55.37	56.21	56.01	56.85	55.32	57.03	55.76	55.48	55.86	56.34
TiO2	0.04	0.05	0.14	0.00	0.00	0.13	0.14	0.13	0.12	0.04	0.13	0.06	0.15	0.13	0.15	0.12
Al2O3	0.71	1.35	3.37	0.78	1.61	3.27	3.07	3.47	3.56	1.45	3.16	2.89	3.77	3.32	3.81	3.12
Cr2O3	0.41	0.47	0.55	0.38	0.46	0.46	0.40	0.56	0.49	0.37	0.46	0.48	0.52	0.51	0.44	0.43
FeOtot	5.95	5.50	6.63	5.78	5.37	6.85	6.59	6.43	6.16	5.39	6.60	6.63	6.45	6.73	6.40	6.31
MnO	0.09	0.10	0.14	0.15	0.20	0.08	0.12	0.11	0.16	0.12	0.08	0.11	0.12	0.10	0.09	0.13
MgO	35.02	35.21	33.16	34.98	35.38	33.05	33.24	33.35	33.37	34.30	32.90	33.81	33.20	33.81	33.22	33.46
CaO	0.62	0.58	0.53	0.60	0.66	0.51	0.41	0.42	0.47	0.58	0.50	0.48	0.51	0.50	0.41	0.46
Na2O	0.02	0.02	0.03	0.03	0.02	0.00	0.02	0.00	0.01	0.04	0.02	0.00	0.00	0.00	0.01	0.00
K2O	0.00	0.00	0.00	0.00	0.00	0.00	0.00	0.00	0.00	0.01	0.00	0.00	0.00	0.00	0.00	0.00
NiO	0.01	0.05	0.08	0.10	0.06	0.05	0.13	0.15	0.04	0.05	0.10	0.09	0.10	0.10	0.12	0.06
Total	99.47	100.46	100.05	100.43	101.22	100.42	99.49	100.83	100.39	99.20	99.27	101.58	100.58	100.68	100.51	100.43
Cation (Structural formula on the basis of 6 oxygen)																
Si	1.96	1.95	1.92	1.97	1.95	1.93	1.92	1.93	1.93	1.97	1.93	1.94	1.92	1.90	1.92	1.94
Ti	0.00	0.00	0.00	0.00	0.00	0.00	0.00	0.00	0.00	0.00	0.00	0.00	0.00	0.00	0.00	0.00
Al	0.03	0.05	0.14	0.03	0.06	0.13	0.13	0.14	0.14	0.06	0.13	0.12	0.15	0.13	0.15	0.13
Fe+3	0.05	0.03	0.01	0.01	0.03	0.00	0.01	0.00	0.00	0.00	0.00	0.00	0.00	0.04	0.00	0.00
Cr+3	0.01	0.01	0.02	0.01	0.01	0.01	0.01	0.02	0.01	0.01	0.01	0.01	0.01	0.01	0.01	0.01
Fe+2	0.12	0.13	0.18	0.15	0.13	0.20	0.18	0.18	0.18	0.16	0.19	0.19	0.19	0.15	0.18	0.18
Mn	0.00	0.00	0.00	0.00	0.01	0.00	0.00	0.00	0.00	0.00	0.00	0.00	0.00	0.00	0.00	0.00
Mg	1.80	1.79	1.71	1.79	1.79	1.70	1.72	1.71	1.71	1.77	1.71	1.72	1.70	1.73	1.70	1.72
Ca	0.02	0.02	0.02	0.02	0.02	0.02	0.02	0.02	0.02	0.02	0.02	0.02	0.02	0.02	0.02	0.02
Na	0.00	0.00	0.00	0.00	0.00	0.00	0.00	0.00	0.00	0.00	0.00	0.00	0.00	0.00	0.00	0.00
K	0.00	0.00	0.00	0.00	0.00	0.00	0.00	0.00	0.00	0.00	0.00	0.00	0.00	0.00	0.00	0.00
Ni	0.00	0.00	0.00	0.00	0.00	0.00	0.00	0.00	0.00	0.00	0.00	0.00	0.00	0.00	0.00	0.00
En	0.92	0.92	0.90	0.91	0.92	0.89	0.90	0.90	0.90	0.91	0.89	0.89	0.89	0.91	0.90	0.90
Fs	0.06	0.07	0.09	0.08	0.06	0.10	0.09	0.10	0.09	0.08	0.10	0.10	0.10	0.08	0.10	0.09
Wo	0.01	0.01	0.01	0.01	0.01	0.01	0.01	0.01	0.01	0.01	0.01	0.01	0.01	0.01	0.01	0.01
Mg#	0.91	0.92	0.90	0.92	0.92	0.90	0.90	0.90	0.91	0.92	0.90	0.90	0.90	0.90	0.90	0.90

from the Kuhshah peridotites indicate that these rocks have been strongly depleted from incompatible elements. Al_2O_3, CaO, and MgO contents (0.27–0.82, 0.37-0.42, 43-46 wt% respectively), along with Ni (2360-2710 ppm) and Cr (2000-3300 ppm) contents from Kuhhsah dunites and harzburgites plot within the range expected for residual peridotites [9]. Kuhshah dunites are slightly more depleted in SiO_2 (37.3-38.8 wt%) and Al_2O_3 (0.15-0.24 wt%) when compared with the harzburgites. The whole rock chemistry of Kuhshah dunites and harzburgites is more depleted than the primary mantle peridotites and deviates from abyssal peridotites in terms of Al_2O_3, CaO, SiO_2 and FeO contents [12].

Olivine–clinopyroxenites show distinctive chondrite-normalized REE patterns (Fig. 6) with light LREE depletion accompanied by relatively low REE abundances. The HREE abundances in the Kuhshah olivine–clinopyroxenites are low (Yb between 0.16 and 0.27 ppm), despite the high modal proportions of

Table 5. Representative analyses of different types of clinopyroxenes from Kuhshah massif.

Sample	Ks7				Ks11			Ks21	Ks22	Ks24	Ks121			Ks133				
Rock	Ol-Cpxt	Ol-Cpxt	Ol-Cpxt	Ol-Cpxt	Ol-Cpxt	Ol-Cpxt	Ol-Cpxt	Ol-Cpxt	Ol-Cpxt	Ol-Cpxt	Ol-Cpxt	Ol-Cpxt	Ol-Cpxt	Ol-Cpxt	Ol-Cpxt	Ol-Cpxt	Ol-Cpxt	Ol-Cpxt
Mineral	Cpx	Cpx	Cpx	Cpx	Cpx	Cpx	Cpx	Cpx	Cpx	Cpx	Cpx	Cpx	Cpx	Cpx	Cpx	Cpx	Cpx	Cpx
SiO2	54.09	53.84	53.77	53.93	52.17	53.77	53.70	53.94	53.88	53.55	53.33	54.06	53.03	52.99	53.38	53.17	53.65	53.26
TiO2	0.09	0.11	0.07	0.12	0.34	0.10	0.09	0.10	0.09	0.08	0.20	0.17	0.20	0.18	0.15	0.11	0.14	0.19
Al2O3	0.47	1.57	0.95	1.03	1.42	1.71	1.88	1.52	1.77	1.85	2.62	2.52	2.50	2.51	2.35	2.62	2.28	2.75
Cr2O3	0.04	0.23	0.52	0.31	0.26	0.52	0.60	0.43	0.58	0.57	0.53	0.44	0.50	0.59	0.66	0.82	0.65	0.57
FeO tot	3.52	3.72	3.20	3.20	5.98	3.46	3.28	2.94	3.52	3.15	3.10	3.18	3.54	3.03	3.38	3.25	3.26	3.32
MnO	0.14	0.10	0.12	0.11	0.52	0.18	0.09	0.10	0.03	0.02	0.09	0.00	0.27	0.24	0.16	0.22	0.00	0.18
MgO	16.70	16.10	16.44	16.45	16.25	16.62	16.51	16.23	16.36	16.60	16.42	16.39	16.27	16.50	16.22	15.86	16.50	16.19
CaO	24.41	24.10	24.55	24.53	22.90	23.94	24.03	24.54	24.65	24.58	24.00	24.01	24.16	24.08	24.41	23.71	23.80	24.28
Na2O	0.39	0.13	0.09	0.08	0.11	0.17	0.18	0.10	0.15	0.13	0.19	0.20	0.17	0.27	0.18	0.17	0.14	0.13
K2O	0.00	0.00	0.00	0.00	0.00	0.00	0.01	0.00	0.00	0.00	0.00	0.02	0.00	0.00	0.01	0.00	0.00	0.00
NiO	0.10	0.00	0.01	0.04	0.00	0.07	0.02	0.00	0.00	0.07	0.00	0.00	0.01	0.01	0.00	0.01	0.00	0.05
Total	99.95	99.90	99.72	99.80	99.95	100.54	100.39	99.90	101.03	100.60	100.48	100.99	100.65	100.40	100.90	99.94	100.42	100.92
Cation (Structural formula on the basis of 6 oxygen)																		
Si	1.97	1.97	1.97	1.97	1.92	1.95	1.95	1.97	1.95	1.94	1.94	1.95	1.93	1.92	1.93	1.95	1.95	1.93
Ti	0.00	0.00	0.00	0.00	0.01	0.00	0.00	0.00	0.00	0.00	0.01	0.00	0.01	0.00	0.00	0.00	0.00	0.01
Al	0.02	0.07	0.04	0.04	0.06	0.07	0.08	0.07	0.08	0.08	0.11	0.11	0.11	0.11	0.10	0.11	0.10	0.12
Fe+3	0.06	0.00	0.00	0.00	0.08	0.01	0.01	0.00	0.01	0.02	0.00	0.00	0.03	0.04	0.02	0.00	0.00	0.01
Cr+3	0.00	0.01	0.02	0.01	0.01	0.01	0.02	0.01	0.02	0.02	0.02	0.01	0.01	0.02	0.02	0.02	0.02	0.02
Fe+2	0.05	0.11	0.09	0.10	0.10	0.09	0.09	0.09	0.09	0.07	0.09	0.10	0.08	0.05	0.08	0.10	0.10	0.09
Mn	0.00	0.00	0.00	0.00	0.02	0.01	0.00	0.00	0.00	0.00	0.00	0.00	0.01	0.01	0.00	0.01	0.00	0.01
Mg	0.91	0.88	0.90	0.90	0.89	0.90	0.89	0.88	0.88	0.90	0.89	0.88	0.88	0.89	0.88	0.87	0.89	0.87
Ca	0.95	0.95	0.96	0.96	0.90	0.93	0.94	0.96	0.96	0.96	0.93	0.93	0.94	0.94	0.95	0.93	0.93	0.94
Na	0.03	0.01	0.01	0.01	0.01	0.01	0.01	0.01	0.01	0.01	0.01	0.01	0.01	0.02	0.01	0.01	0.01	0.01
K	0.00	0.00	0.00	0.00	0.00	0.00	0.00	0.00	0.00	0.00	0.00	0.00	0.00	0.00	0.00	0.00	0.00	0.00
Ni	0.00	0.00	0.00	0.00	0.00	0.00	0.00	0.00	0.00	0.00	0.00	0.00	0.00	0.00	0.00	0.00	0.00	0.00
En	0.47	0.45	0.46	0.46	0.47	0.47	0.46	0.46	0.46	0.47	0.46	0.46	0.46	0.47	0.46	0.46	0.47	0.46
Fs	0.03	0.06	0.05	0.05	0.05	0.05	0.05	0.05	0.05	0.04	0.05	0.05	0.04	0.03	0.04	0.05	0.05	0.05
Wo	0.50	0.49	0.49	0.49	0.48	0.48	0.49	0.50	0.50	0.50	0.49	0.49	0.50	0.50	0.50	0.49	0.48	0.49

Table 6. Whole rock analyses of Kuhshah peridotites.

sample	Ks2	Ks3	Ks10	Ks1	Ks6	Ks12	Ks25	Ks7	Ks11	Ks21	Ks22	Ks24	Ks27	Ks121	Ks133
Rock type	Du	Du	Du	Hz	Hz	Hz	Hz	Ol-Cpxt	Ol-Cpxt	Ol-Cpxt	Ol-Cpxt	Ol-Cpxt	Ol-Cpxt	Ol-Cpxt	Ol-Cpxt
SiO2	37.4	37.3	38.8	42.5	42.2	42.6	41.2	51.5	53.63	53.21	49.12	50.12	50.73	48.32	49.6
TiO2	0.01	0.02	0.02	0.01	0.02	0.02	0.01	0.08	0.08	0.1	0.11	0.11	0.08	0.11	0.1
Al2O3	0.17	0.15	0.24	0.62	0.82	0.27	0.43	2.91	2.81	3.13	2.8	2.93	3.21	2.63	3.12
FeOtot	8.26	8.73	9.76	7.86	8.01	7.22	8.46	4.83	4.76	5.31	5.03	5.61	5.38	4.8	3.56
MnO	0.11	0.14	0.13	0.1	0.11	0.12	0.11	0.12	0.21	0.11	0.11	0.21	0.25	0.13	0.12
MgO	44.6	44.3	44.2	43.2	46.43	45.32	44.65	24.35	23.65	19.86	20.31	23.2	23.65	26.35	25.83
CaO	0.61	0.53	0.16	0.37	0.42	0.4	0.38	14.65	14.73	15.6	14.93	16.34	15.38	16.04	15.64
Na2O	0.02	0.01	0.01	0.01	0.02	0.01	0.01	0.08	0.11	0.38	0.41	0.11	0.18	0.09	0.34
K2O	< 0.01	< 0.01	< 0.01	< 0.01	< 0.01	< 0.01	< 0.01	< 0.01	< 0.01	< 0.01	< 0.01	< 0.01	< 0.01	< 0.01	< 0.01
LOI	8.32	9.02	6.98	4.83	1.77	4.04	4.55	1.38	0.62	2	6.98	1.87	1.54	1.73	1.39
Total	99.5	100.2	100.3	99.5	99.8	100	99.8	99.9	100.6	99.7	99.8	100.5	100.4	100.2	99.7
ppm															
Nb	0.25	0.2	< 0.2	0.2	< 0.2	< 0.2	< 0.2	0.33	0.3	0.2	< 0.2	< 0.2	< 0.2	0.29	0.21
Zr	3	3	3	3	22	< 2	2	2	2	2	2	2	2	< 2	< 2
Y	0.5	1	< 0.5	1.5	1	< 0.5	1	2.6	2.8	2.5	2.7	3.2	3.1	1.9	3.8
Sr	7.8	7.4	3	3.2	4.1	1.2	1.6	7.3	9.6	7.4	9	9.3	21.3	11	7.6
Rb	0.3	0.5	0.7	0.3	0.4	0.3	0.7	1	0.3	0.3	0.4	0.2	0.3	0.2	0.2
Ga	3	0.2	2.4	0.8	0.9	2.3	2.4	3	3.2	2.6	2	3.5	3	3.3	2
Zn	28	25	21	51	53	49	55	30	31	26	29	31	30	25	26
Ni	2550	2200	2370	2650	2360	2710	2640	865	365	315	825	530	445	720	475
Co	125.5	118	87.5	120	115	118.5	113.5	45	61.5	53.3	58.3	56.3	48.2	60.3	48.2
Cr	2600	2860	3100	3300	2880	3150	2930	3460	4350	4860	6050	3960	4730	6180	5930
V	50	20	40	20	36	13	24	53	68	56	63	74	71	70	56
La	< 0.5	< 0.5	< 0.5	< 0.5	< 0.5	< 0.5	< 0.5	< 0.5	< 0.5	< 0.5	< 0.5	< 0.5	< 0.5	< 0.5	< 0.5
Ce	< 0.5	< 0.5	< 0.5	< 0.5	< 0.5	< 0.5	< 0.5	< 0.5	< 0.5	< 0.5	< 0.5	< 0.5	< 0.5	< 0.5	< 0.5
Pr	< 0.03	< 0.03	< 0.03	< 0.03	< 0.03	< 0.03	< 0.03	0.04	0.08	0.05	0.06	0.07	0.07	0.05	0.05
Nd	< 0.1	< 0.1	< 0.1	< 0.1	0.1	0.1	< 0.1	0.35	0.38	0.5	0.45	0.47	0.5	0.61	0.54
Sm	< 0.03	< 0.03	< 0.03	< 0.03	0.06	0.09	< 0.03	0.16	0.21	0.2	0.22	0.16	0.28	0.16	0.17
Eu	< 0.03	< 0.03	< 0.03	0.04	< 0.03	0.05	< 0.03	0.07	0.11	0.08	0.06	0.09	0.09	0.09	0.08
Gd	< 0.05	< 0.05	< 0.05	0.1	0.1	< 0.05	< 0.05	0.28	0.41	0.27	0.4	0.38	0.51	0.33	0.36
Tb	0.01	0.01	0.01	0.01	0.03	0.04	0.01	0.08	0.07	0.07	0.11	0.6	0.07	0.09	0.06
Dy	< 0.05	< 0.05	< 0.05	0.1	0.21	0.16	< 0.05	0.38	0.46	0.45	0.49	0.37	0.33	0.68	0.49
Ho	0.01	< 0.01	0.01	0.01	0.04	0.05	0.01	0.09	0.08	0.09	0.07	0.07	0.09	0.11	0.06
Er	< 0.03	< 0.03	< 0.03	0.03	0.15	0.18	0.03	0.28	0.19	0.19	0.26	0.28	0.2	0.27	0.21
Yb	0.03	< 0.03	< 0.03	0.04	0.05	0.04	0.03	0.26	0.16	0.26	0.27	0.19	0.24	0.16	0.25
Lu	0.01	0.02	0.02	0.03	0.01	0.01	0.02	0.04	0.04	0.02	0.03	0.02	0.04	0.04	0.03

clinopyroxene. These rocks have convex upward REE pattern with depleted LREE relative to MREE and relatively flat HREE-MREE gradients [$(Gd/Yb)_N$ ~1].

Discussion

Evidence derived from the field, petrography, mineral chemistry and whole rock chemical studies show that the Kuhshah peridotites, like several well-known peridotite suits [17,1,21], underwent chemical modification caused by melt/rock reaction after depletion by partial melting. In Kuhshah, these evidences include: (1) Kuhshah Harzburgites differ from abyssal peridotites [34,35] by lower Al_2O_3 and SiO2 and higher MgO contents (Table 6); (2) Mineral compositions in Kuhshah peridotites do not show a simple partial melting event of the mantle (Figs. 4a); (3) Presence of several generations of olivine, orthopyroxene and spinel (Tables 2-4 and Fig. 4c); (4) Spinels in Kuhshah peridotites display high Cr # (>0.5). These high Cr # values may reflect high degrees of partial melting in the mantle [12] or interaction between percolating melts and mantle peridotites [27]. Therefore, first, we discuss partial melting events in the Kuhshah peridotites.

Partial melting of peridotites

Low proportions of clinopyroxene in mantle peridotites (e.g., Kuhshah) are generally interpreted to signify extensive melting [12]. But in Kuhshah, there are petrographic (Fig. 3f) and mineral chemistry (Table 4) evidences showing that both orthopyroxene (Opx1) and clinopyroxene melted during partial melting of Kuhshah mantle peridotite and this event must have taken place in a special tectonic setting in which orthopyroxene can also melt incongruently. Above subduction zones, decompression melting is facilitated by the presence of H_2O derived from the subducted slab [55]. Moreover, H_2O favours incongruent melting of orthopyroxene, generating olivine + chromespinel as found in Kuhshah harzburgites (Fig. 3f). Dick *et al*. [13] argued that the clinopyroxene content of peridotites is a measure of the degree of depletion. On these criteria, Kuhshah harzburgites are highly depleted (<2 vol % clinopyroxene). There are some mineral chemical signatures consistent with partial melting in the harzburgites. For example, Kuhshah olivines from harzburgites (Ol1) contain high forsterite contents (0.92-0.93), typical of residual mantle [5]. Moreover, these olivines exhibit higher NiO contents (Table 2) compared with those of dunites and overlap the mantle olivine array, showing a residual origin for these rocks. The Cr # of primitive harzburgitic spinels in Kuhshah

Table 7. Geological evidences in favor of suprasubduction zone affinity on Kuhshah peridotites.

Evidences	Indicated tectonic setting	Preferences/This study
Fe2O3 vs TiO2 (wt%) in spinel	Suprasubduction zone setting	Bridges et al., (1995)/ 12a
Cr# (spinel) vs Mg# (olivine)	Suprasubduction zone setting	Pearce et al., (2000)/ 12b
TiO2 vs Al2O3 (wt%) in spinel	Suprasubduction zone setting	Kamentskey et al.,2001/ 12c
ΔfO_2 vs Cr# in spinel	Suprasubduction zone peridotites	Dare et al., (2009)
Cr# vs Mg# in spinel	Abyssal peridotites	Batanova et al., (2005)
Cr# (spinel) vs Fo-number (olivine)	Alpine type peridotites	Arai and Matsukage (1998)
Cr# vs Mg# in spinel	Alpine type peridotites	Arif (2006)
Cr# vs Mg# in spinel	Suprasubduction zone peridotites	Parkinson and Pearce (1998)
Al-Cr-Fe^{3+} in spinel	Residual peridotites of ophiolites	Arif (2006)
Cr# vs Mg# in spinel	MORB	Ravikant et al., (2004)
Fe^{2+} /Fe^{3+} vs Al2O3 (wt%) in spinel	Suprasubduction zone peridotites	Kamentskey et al.,2001
Cr# vs Mg# in spinel	Suprasubduction zone ophiolites	Bridges et al., (1995)

(Sp1), relative to experimental data of Hiorse and Kawamoto [20], indicates 20% partial melting for the host rocks. According to the partial melting model proposed by Pearce *et al*. [39], based on Yb versus V diagram, Kuhshah harzburgites were generated by 20-25% partial melting. High Ni and Cr concentrations (2590 and 3065 ppm respectively) in Kuhshah rocks, high forsterite contents of primary olivines (Ol1) (an average of 0.925), high Cr # of spinel (0.705) and curve-shaped contacts of the first generation minerals, all suggest that Kuhshah harzburgites are refractory mantle residues.

The lobate boundaries, which are commonly observed in Kuhshah orthopyroxenes (Opx1), are interpreted as resorption features associated with the incongruent melting of orthopyroxenes [37]. The higher values of Cr-numbers in some spinels from Kuhshah peridotites (Sp1 in Table 3) relative to the abyssal spinel peridotites that reported by Hellebrand et al.,[19] and Warren and Shimizu, [57] reflect the refractory origin for these rocks.

Aspects of melt/peridotite reactions

In Kuhshah harzburgites, there are lines of evidence for melt/rock reaction such as; orthopyroxene dissolution-secondary olivine formation, interstitial crystallization of orthopyroxene and different generations of spinel. Moreover, second generation of Kuhshah orthopyroxenes (Opx2) can be formed from certain ascending melts in mantle conditions, or replaced primary olivines due to melt/rock interaction [5]. All of these features can relate to the melt/rock reaction events. Mineralogical features showing the occurrence of theses multi-stage events in Kuhshah peridotites are as follows:

Harzbugite–dunite transformation can occur due to a pyroxene consuming-olivine forming reaction process (as shown in Fig. 3b). This reaction implies infiltration of a silica undersaturated melt, and has an important role in the formation of replacive dunite bodies [58,24]. Such a reaction can also affect the earlier spinels and produces spinels that are compositionally similar to dunitic spinels. So this type of spinels (chrome-rich) in Kuhshah dunites can form by the following reaction:

Al-rich spinel + liquid 1 = Cr-spinel (more rich in chrome) + liquid 2

Following this reaction, residual Sp1 from harzburgites is replaced by more chromian and relatively Ti-rich spinel in dunites [59]. As illustrated in Figure 7, dunites may have been produced by channeled reactive migration of boninitic melts trough the depleted harzburgites. According to this figure, Kuhshah dunites can be produced by the reaction of refractory harzburgites (with almost 20% fusion) with boninitic melts, because both dunites and harzburgites follow the trend of reaction toward boninites. Gradually, due to continued dissolution of pyroxenes, percolating melts are enriched in Si and Cr and in the next stage, at shallower depths, interstitial orthopyroxene (Opx2 in Fig. 3d), spinel and chromitite bands crystallize. In this stage, reverse reaction can take place as:

Olivine + Melt 1 = Orthopyroxene (Opx 2) + Spinel 2 + melt 2

The relatively low contents of CaO, Al_2O_3 and Cr_2O_3 in Opx2 from Kuhshah (0.6, 0.47 and 0.43 in average respectively) are similar to secondary orthopyroxenes that is interpreted to have formed by metasomatism by aqueous fluids of slab origin [5]. In Kuhshah harzburgites, interstitial exsolution free undeformed orthopyroxenes (Opx2) and Sp2 have been aligned along the contacts with olivines (Fig. 3d) and/or cross-cutting larger porphyroblastic ones.

According to the Ol-Cr-Q phase diagram (Fig. 8) from Irvine [23], in Kuhshah massif, primitive melt (A) that has been originated in the deeper levels from partial melting of the harzburgites, may reacts with host peridotites and its composition moves along interaction trend to form the chromitite bands and the dunites. So, the dunites and chromitites are subsequent to the harzburgites. This is evident by irregular and patchy

shapes of dunites that clearly cut the banding of the harzburgites. Then, the remaining melt ascends into upper harzburgites and its composition migrates toward orthopyroxene-chromite cotectic (point C), and in the upper levels of the Kuhshah massif, accessory Opx2 crystallizes in impregnated harzburgites. Chemically, Opx2 is characterized by relatively low contents of CaO, Al_2O3 and Cr_2O_3 relative to the Opx1, but similar Mg# (Table 4). These features are maintained by aqueous fluids or H_2O-rich melts in the mantle wedge above subduction zones [6,56]. The NiO content of olivines from Kuhshah harzburgites (Ol1) varies from 0.14-0.55 wt%. This range is beyond the ordinary NiO range (0.3-0.4) in mantle harzburgites [4]. Moreover, the variation of Fo contents of olivines (Ol1, Ol2 and Ol3) from Kuhshah harzburgites is large (88-93).This range which covers all of the mantle peridotites [4], can be found in Kuhshah harzburgites and some of these olivines may have been produced by interaction of depleted harzburgites with ascending melts. These melts can crystallize the second generation olivines (Ol2) with lower contents of NiO and fo-no in compare with the primary olivines.

It is most likely that Kuhshah dunites have been produced from depleted harzburgites due to melt/rock interaction, where the migrating melts have focused and retained as melt pockets, or some dunites were channels through which percolating melts ascent and caused incongruent melting of orthopyroxenes (Opx1) [27]. Pearce *et al*. [39] stated that if dunites are produced by multistage partial melting, their spinels must contain TiO_2 <0.1 wt %, and if melt/harzburgite reactions produce dunites, the TiO_2 content is almost 0.2 wt %. In Kuhshah dunitic spinels, TiO_2 contents range between 0.21 and 0.24 wt%. So, these chemical features for Kuhshah dunites are probably related to the interaction of the peridotites with ascending magmas. In the MORB ophiolites, dunitic channels can produced by interaction between peridotites and ascending MORB melts [27], but in suprasubduction zone settings, many researchers [37,41,5] believe subduction related magmas can play such a role. Chemical composition of cr-spinel in Kuhshah chromitites and related dunites are completely different from Sp1 of the harzburgites. The Ti content is 4-6 times higher in spinels of the chromitites and dunites than in Sp1 of harzburgites. This suggests that harzburgite-dunite-chromitites of Kuhshah have not comagmatic origin. Spinel chemistry is almost the same in the chromitite bands and related dunites, exept for Mg ratio that may have been changed during subsolidus reactions. Thus it is most probably that Kuhshah dunites and chromitite bands are comagmatic.

Olivine-clinopyroxenite intrusives

In many ultramafic massifs, there are pyroxenitic dykes or bands that are emplaced parallel or subparallel to the foliation of host peridotites and several mechanisms are proposed for the origin of these rocks [53,49,15,47].

Kuhshah clinopyroxenites are found as dykes and veins and show cumulative texture. Since these intrusives follow the main fractures and cut all of the units, they can not be involved in the earlier pervasive melt/rock interaction processes and formation of Kuhshah dunites and chromitites. In addition, olivine composition in these rocks is completely different from those in harzburgites and dunites (Table 2), however in Fig. 5b, clinopyroxenes from olivine-clinopyroxenites plot in the field of mantle pyroxenites.

Kuhshah clinopyroxenites show depleted LREE patterns (Fig. 6) consistent with formation via partial melting of depleted mantle source. Low concentrations of incompatible elements such as Ti and Na_2O in clinopyroxenes of these rocks (Table 5) suggest that low Al parental melts have derived from those parts of the mantle which have been depleted in basaltic components previously. However, non-primitive Mg-number (0.81-0.85) of olivines suggests that the melts have probably evolved by fractional crystallization from more primitive mantle melts. Parlak *et al*. [38] argued that the presence of highly magnesian clinopyroxene together with the absence of plagioclase in pyroxenites, indicate the rocks can be formed through moderate to high pressure (up to 10 kb) crystal fractionation of primary basaltic melts. Depletion of HFSE, high Si and Mg and low Al contents - as shown in Table 6 - are similar to those melts (boninites) that show chemical variations due to the influence of suprasubduction zone setting. Such boninitic melts are found in modern and ancient subduction zone environments [29]. The presence of melts from which the olivine-clinopyroxenites have crystallized, indicate that the refractory sub-arc mantle was reactivated and contributed to magma genesis. Remelting of refractory arc mantle requires a high temperature thermal regime and/or a lowering of the peridotite solidus [29]. In Kuhshah massif, the latter case is more probable, and decrease of pressure due to updoming may be more important. Shahabpour [50], based on the geophysical evidences demonstrated that in south-east Sanandaj-Sirjan zone, mantle has drastically updomed. In Kuhshah massif, some of these intrusives are parallel to- and the others cut the foliation of host rocks suggesting the injection of the melts were contemporaneous with the diapiric ascent of the mantle and therefore, they are syn-uplift intrusive rocks.

Tectonic setting

It has been shown that most of the ophiolite sequences come from suprasubduction zone (SSZ), [46,7,54,6]. It has been noted by many authors that the mantle peridotites beneath arc setting are expected to be more depleted in magmatic components than those from other tectonic settings, especially MOR. But the whole chemistry and mineralogy of these complexes can not be interpreted simply by a partial melting event; because, they have experienced variable extent of metasomatism by hydrous melts within the suprasubduction zone mantle wedge. Many evidences have been presented that indicate Eastern Mediterranean ophiolites formed in suprasubduction zone setting. For example, Parlak *et al*. [38] showed Pozanti-Karsanti ophiolite (Turkey) has been originated in such environment during the closure of Neotethys, sometimes in late Cretaceous. Inwood *et al*. [22] presented a paleomagnetic analysis of the upper Cretaceous Hatay (Kizildag) ophiolite in Turkey and stated this ophiolite formed in the same suprasubductuion zone spreading system as the Troodos ophiolite (Cyprus). Moreover, Dilek and Thy [14] stated that Hatay ophiolite is part of a peri-Arabian ophiolitic belt in the eastern Mediterranean region, including the Troodos, Baer-Basit (Syria) and Semail (Oman) ophiolites. They demonstrated that in this ophiolite, similar to most Tethyan ophiolites, there is multi-stage suprasubduction zone magmatism that is analogous to the earlier arc volcanism in the Eocene-Oligocene Izu-Bonin Mariana system. Shahabpour [51] presented the Shahrebabak-Baft ophiolites and the back arc basin environment (BAB) in southern Sanandaj-Sirjan zone, proposing a high angle subduction zone in this region: so that, at Cretceous period, Sanandaj-Sirjan zone acted as an island arc. This situation could be associated with the petrological processes that normally take place in suprasubduction zone setting. Chemical compositions of spinels in Kuhshah also confirm this geological environment for the host rocks (Fig. 9a). It is probable that the Kuhshah peridotites have been partially melted in a back arc basin due to mantle upwelling and decompression, and their composition has been resembled to the MORB type peridotites. Then, suprasubduction zone related processes affected them and the composition of spinels changed toward those spinels which are found in SSZ. This process is indicated by the continuous chemical trend of Kuhshah spinels from MOR-type to suprasubduction zone peridotites in Figure 9b.

Conclusions

1) There are some evidences in Kuhshah peridotites that show their primary rocks have been originated in a back arc basin.

2) The primary depleted harzburgites, underwent several stages of melt/rock interaction at spinel facies condition and Kuhshah dunites mainly formed due to melt/peridotite reaction and incongruent melting of orthopyroxene.

3) The chromitite bands have been formed from suprasubduction zone related boninitic melts.

4) The parental melts of olivine-clinopyroxenites have been formed in mantle wedge well after the pervasive melt/rock reaction and migrated upward during the uplift of the lithosphere.

5) These events could have occurred in a suprasubduction zone setting, where Neotethys plate subducted beneath the Sanandaj-Sirjan zone, and a back-arc basin that had newly formed between Sanandaj-Sirjan zone and central Iranian microcontinent.

6) Final emplacement of Kuhshah massif in the Sanandaj-Sirjan metamorphic rocks occurred in solid state condition as a hot crystalline mass.

References

1. Agashev A.M., Ionov D.A., Pokhilenko N.P., Golovin A.V., Cherepanova Yu., and Sharygin I.S., Metasomatism in lithospheric mantle roots: Constraints from whole-rock and mineral chemical composition of deformed peridotite xenoliths from kimberlite pipe Udachnaya. *Lithos*, **160–161**: 201-215 (2013).
2. Arai S., Chemistry of chromian spinel in volcanic rocks as a potential guide to magma chemistry. *Mineral. Mag.*, **56**: 173-184 (1992).
3. Arai S., Compositional variation of olivine-chromian spinel in Mg-rich magmas as a guide to their residual spinel peridotites. *J. Volcanol. Geotherm. Res.*, **59**: 279-293 (1994a).
4. Arai S., Characterization of spinel peridotites by olivine-spinel compositional relationships: Review and interpretation. *Chem. Geol.*, **113**: 191-204 (1994b)
5. Arai S., Ishimaru S. and Okrugin V.M., Metasomatized harzburgite xenoliths from Avacha Volcano as fragments of mantle wedge of the Kamchatka arc: an implication for the metasomatic agent. *Island Arc*, **12**: 233-246 (2003).
6. Arai S. and Ishimaru S., Insights onto petrological characteristics of the lithosphere of mantle wedge beneath arcs through peridotite xenoliths: a review. *J. Petrol.*, **49**(4): 665-695 (2008).
7. Beccaluva L., Coltorti M., Saccani E. and Siena F., Magma generation and crustal accretion as evidence by suprasubduction ophiolites of the Albanide-Helenide Subpelagonian Zone. *Island Arc*, **14**: 551-563 (2005).
8. Berly T.S., Hermann J., Arculus R.J. and Lapierre H., Supra-subduction zone pyroxenites from San Jorge and Santa Isabel (Solomon Islands). *J. Petrol.*, **47**(8): 1531-1555

(2006).
9. Brown G.C. and Mussett A.E., The inaccessible earth: an integrated view to its structure and composition. Xi. *Chapman and Hall*, London, New York. 276 p (1993) .
10. Brueckner H.K. and Medaris L.G., A general model for the intrusion and evolution of mantle garnet peridotites in high pressure and ultra-high pressure metamorphic terranes. *J. Metamorph. Geol.*, **18**: 123-133 (2000).
11. Dare S.A.S., Pearce J.A., McDonald I. and Styles T., Tectonic discrimination of peridotites using fO2 –Cr# and Ga-Ti-Fe^{3+} systematics in chrome-spinel. *Chem. Geol.*, **261**: 199-216 (2009).
12. Dick H.J.B. and Bullen T., Chromian spinel as a petrogenetic indicator in abyssal and alpine type peridotites and spatially associated lavas. *Contrib. Mineral. Petrol.*, **86**: 54-76 (1984).
13. Dick H.J.B., Fisher R.L. and Bryan W.B., Mineralogic variability of the uppermost mantle along mid ocean ridges. *Earth Planet. Sci. Lett.*, **69**: 88-106 (1984).
14. Dilek Y. and Thy P., Island arc tholeiite to boninitic melt evolution of the Cretaceous Kizildag (Turkey) ophiolite: Model for multi-stage early arc-forearc magmatism in Tethyan subduction factories. *Lithos*, **113**: 68-87 (2009).
15. Downes H., Formation and modification of the shallow sub-continental lithospheric mantle: A review of geochemical evidence from ultramafic xenolith suites and tectonically emplaced ultramafic massifs of Western and Central Europe. *J. Petrol.*, **42**(1): 233-250 (2001).
16. Ghasemi A. and Talbot C.J., A new tectonic scenario for the Sanandaj-Sirjan zone (Iran). *J. Asian Earth Sci.*, **26**(6): 638-693 (2006).
17. González-Jiménez J.M., Marchesi C., Griffin W.L., Gutiérrez-Narbona R., Lorand J.P., O'Reilly S.Y., Garrido C.J., Gervilla F., Pearson N.J., and Hidas K., Transfer of Os isotopic signatures from peridotite to chromitite in the subcontinental mantle: Insights from in situ analysis of platinum-group and base-metal minerals (Ojénperidotite massif, southern Spain). *Lithos*, **164–167**: 74–85 (2013).
18. Hassanipak A.A., Ghazi A.M. and Wampler J.M., REE characteristics and K/Ar ages of the BandZiarat opiolite complex, south-eastern Iran. *Can. J. Earth, Sci.*, **33**: 1534-1542 (1996).
19. Hellebrand E., Snow J.E. and Mühe R., Mantle melting beneath Gakkel Ridge (Arctic Ocean): abyssal peridotite spinel compositions. *Chem. Geol.*, **182**: 227-235 (2002).
20. Hiorse K., Kawatomo T., Hydrous partial melting of lherzolite at 1 Gpa: the effect of H2O on the genesis of basaltic magmas. *Earth Planet. Sci. Lett.*, **133**: 463-473 (1995).
21. Hong L.B., Xu Y.G., Ren Z.Y., Kuang Y.S., Zhang Y.L., Li J., Wang F.Y., Zhang H., Petrology, geochemistry and Re–Os isotopes of peridotite xenoliths from Yantai, Shandong Province: Evidence for Phanerozoic lithospheric mantle beneath eastern North China Craton. *Lithos*, **155**: 256–271 (2012).
22. Inwood J., Morris A., Anderson M.W., Robertson A.H.F., Neotethyan intraoceanic microplate rotation and variations in spreading axis orientation: Palaeomagnetic evidence from the Hatay ophiolite (Southern Turkey). *Earth Planet. Sci. Lett.*, **280**: 105-117 (2009).
23. Irvine T.N., Origin of chromitite layers in the Muskox intrusion and other intrusions: a new interpretation. *Geology*, **5**: 273-277 (1977).
24. Jagoutz O., Muntener O., Ulmer P., Pettke T., Burge J.P., Dawood H., Hussain S., Petrology and mineral chemistry of lower crustal intrusions: The Chilas Complex, Kuhistan (NW Pakistan). *J. Petrol.*, **48**(10): 1895-1953 (2007).
25. Kamenetsky V.S., Sobolov A.V., Eggins S.M., Crowford A.J., Arculus R.J., Olivine-enriched melt inclusions in chromites from low-Ca boninites, Cape Vogel, Papua New Guinea: evidence for ultramafic primary magma, refractory mantle source and enriched components. *Chem. Geol.*, **183**: 287-303 (2002).
26. Kelemen P.B., Dick H.J.B., Quick J.E., Formation of harzbugite by pervasive melt-rock reaction in the upper mantle. *Nature*, **358**: 635-641 (1992).
27. Kelemen P.B., Dick H.J.B., Focused melt flow and localized deformation in the upper mantle: juxtaposition of replacive dunite and ductile shear zones in the Josephine ophiolite, SW Oregon. *J. Geophysic. Res.*, **100**: 423-438 (1995).
28. Kepezhinskas P.K., Defant M.J., Drummond M.S., Na metasomatism in the island arc mantle by slab melt peridotite interaction: evidence from mantle xenoliths in the north Kamchatka arc. *J. Petrol.*, **36**: 1505-1527 (1995).
29. Kurth-velz M., Sassen A., Galer S.J.G., Geochemical and isotopic heterogeneties along an island arc-spreading ridge intersection: Evidence from the Lewis Hill, Bay of Island Ophiolite, Newfoundland. *J. Petrol.*, **45**(3): 635-668 (2004).
30. McCall G.J.H., The geotectonic history of the Makran and adjacent areas of Southern Iran. *J. Asian Earth Sci.*, **15**(6): 517-531 (1998).
31. Medaris L.G., High pressure peridotites in south-western Oregon. *Bull. Geologic. Soc. Am.*, **83**: 41-58 (1972).
32. Mercier J.C.C., Nicolas A., Textures and fabrics of upper mantle peridotites as illustrated by xenoliths from basalts. *J. Petrol.*, **16**: 454-487 (1975).
33. Najafzadeh A.R., Arvin M., Pan Y., Ahmadipour H., Podiform chromitites in the Sorkhband ultramafic complex, Southern Iran: Evidence for ophiolitic chromitite. *J. Sci., Islam. Repub. Iran*, **19**(1): 49-65 (2008).
34. Niu Y., Mantle melting and melt extraction processes beneath ocean ridges: evidence from Abyssal Peridotites. *J. Petrol.*, **38** (8): 1047–1074 (1997).
35. Niu Y., Bulk-rock major and trace element compositions of abyssal peridotites: implications for mantle melting, melt extraction and post-melting processes beneath mid-ocean ridges. *J. Petrol.*, **45**(12): 2423-2458 (2004).
36. Pal T., Mitra S., P-T-fO2 controls on a partly inverse chromite bearing ultramafic intrusive: an evaluation from the Sukinda Massif, India. *J. Asian Earth Sci.*, **22**: 483- 493 (2004).
37. Parkinson I.J., Pearce J.A., Peridotites from Izu-Bonin-Mariana Forearc (ODP Leg 125): Evidence for mantle melting and melt-mantle interaction in a supra-subduction zone setting. *J. Petrol.*, **39**(9): 1577-1618 (1998).
38. Parlak O., Hock V., Delaloye M., The supra-subduction zone Pozanti-Karsanti ophiolite, southern Turkey: Evidence for high-pressure crystal fractionation of ultramafic cumulates. *Lithos*, **65**: 205-224 (2002).
39. Pearce J.A., Barker P.F., Edwards S.J., Parkinson I.J., Leat P.T., Geochemistry and tectonic significance of peridotites

from the South Sandwich arc basin system, South Atlantic. *Contrib. Mineral. Petrol.*, **139**: 36-53 (2000).
40. Pelletier L., Vils F., Kalt A., Gmeling K., Li, Bi and Be contents of harzburgites from the Dramala Complex (Pindos ophiolite, Greece): Evidence for a MOR-type mantle in a supra-subduction zone environment. *J. Petrol.*, **49**(1): 2043-2080 (2008).
41. Peslier A.H., Francis D., Ludden J., The lithospheric mantle beneath continental margins: Melting and melt-rock reaction in Canadian Cordillera xenoliths. *J. Petrol.*, **43**(11): 2013-2047 (2002).
42. Robertson A., Development of concepts concerning the genesis and emplacement of Tethyan ophiolites in the Eastern Mediterranean and Oman regions. *Earth Sci. Rev.*, **66**: 331-387 (2004).
43. Roeder P.L., Campbell I.H., Jamison H.E., Re-evaluation of the olivine-spinel geothermometer. *Contrib. Mineral. Petrol.*, **68**: 325-334 (1979).
44. Sabzehei M., Les mélanges ophiolitiques de la region d'Esfandagheh. These d'etate, *Universite´ scientifique et medicale de Grenoble, France*, 306p (1974).
45. Sabzehei M., Upper protrozoic-lower Paleozoic ultramafic mafic associations of southeast Iran, production of an ophiolitic magma of komatiitic affinity. *Inter. Ophiolite Symp. Finland* (1998).
46. Saccani E., Photiades A., Mid-Ocean Ridge and suprasubduction affinities in the Pindos Ophiolite (Greece): Implications for magma genesis in forearc setting. *Lithos*, **73**: 229-253 (2004)
47. Santos J.F., Scharer U., Ibarguchi J.I.G., Girardeau J., Genesis of pyroxenite-rich peridotite at Cabo Ortegal (NW Spain): geochemical and Pb-Sr-Nd isotope data. *J. Petrol.*, **43**(1): 17-43 (2002).
48. Sengor A.M.C., A new model for the late Paleozoic-Mesozoic tectonic evolution of Iran and implication for Oman. In: Robertson AH F Searle MP Ries AC (Eds) The geology and tectonics of the Oman region. *Geol. Soc. London, Special pub.*, **49**: 797-831 (1990).
49. Seyler M., Paquette J.L., Ceuleneer G., Kienast J.R., Loubet M., Magmatic underplating, metamorphic evolution and ductile shearing in a Mesozoic lower crustal- upper mantle unit (Tinaquillo, Venezuela of the Caribean belt). *J. Geol.*, **106**: 35-58 (1998).
50. Shahabpour J., The role of deep structures in the distribution of some major ore deposits in Iran, NE of the Zagros thrust zone. *J. Geodynamics.*, **28**: 237-250 (1999).
51. Shahabpour J., Tectonic evolution of the orogenic belt in the region located between Kerman and Neyriz. *J. Asian Earth Sci.*, **24**: 405-417 (2005).
52. Soustelle V., Tommasi A., Bodinier J.L., Garido G.J., Vauches A., Deformation and reactive melt transport in the mantle lithosphere above a large-scale partial melting domain: the Ronda peridotite massif, Southern Spain. *J. Petrol.*, **50**(7): 1235-1266 (2009).
53. Suen C.J., Frey F.A., Origins of the mafic and ultramafic rocks in the Ronda peridotite. *Earth Planet. Sci. Lett.*, **85**: 183-202 (1987).
54. Tamura A., Arai S., Harzburgite-dunite-orthopyroxenite suite as a record of supra-subduction zone setting for the Oman ophiolite mantle. *Lithos*, **90**: 43-56 (2006).
55. Tatsumi Y., Eggins S., Subduction zone magmatism. *Blackwell, Cambridge* 211 p (1995).
56. Uysal I., Ersoy E.Y., Karsli O., Dilek Y., Sadiklar M.B., Ottley C.J., Tiepolo M., and Meisel T., Coexistence of abyssal and ultra-depleted SSZ type mantle peridotites in a Neo-TethyanOphiolite in SW Turkey: Constraints from mineral composition, whole-rock geochemistry (major–trace–REE–PGE), and Re–Os isotope systematics. *Lithos*, **132–133**: 50–69 (2012).
57. Warren J.M. and Shimizu N., Cryptic variations in abyssal peridotite compositions: evidence for shallow-level melt infiltration in the oceanic lithosphere. *J. Petrol.*, **51**(1 &2): 395-423 (2010).
58. Witt-Eickschen G., Seck H.A., Mezger K., Eggins S.M., Altherr R., Lithospheric mantle evolution beneath the Eifel (Germany): Constraints from Sr-Nd-Pb isotopes and trace element abundances in spinel peridotite and pyroxenite xenoliths. *J. Petrol.*, **44**(6): 1077-1095 (2003).
59. Zhou M.F., Robinson P.T., Malpas J., Li Z., Podiform chromitites in the Loubusa ophiolite (Southern Tibet): implications for melt-rock interaction and chromite segregation in the upper mantle. *J. Petrol.*, **37**(1): 3-21 (1996).
60. Zhou M.F., Robinson P.T., Malpas J., Edwards S.J., Qi L., REE and PGE geochemical constraints on the formation of dunites in the Luobusa ophiolite, Southern Tibet. *J. Petrol*., **46**(3): 615-639 (2005).